ACS APPLIED MATERIALS & INTERFACES

LETTER

www.acsami.org

Noncovalent Functionalization of Disentangled Boron Nitride Nanotubes with Flavin Mononucleotides for Strong and Stable Visible-Light Emission in Aqueous Solution

Zhenghong Gao,[†] Chunyi Zhi,[‡] Yoshio Bando,[‡] Dmitri Golberg,[‡] and Takeshi Serizawa*[,§]

[†]Department of Advanced Interdisciplinary Studies, Graduate School of Engineering, and [§]Research Center for Advanced Science and Technology, The University of Tokyo, 4-6-1 Komaba, Meguro-ku, Tokyo, 153-8904, Japan,

[‡]International Center for Materials Nanoarchitectonics (MANA), National Institute for Materials Science (NIMS), Namiki 1-1, Tsukuba, Ibaraki 305-0044, Japan, and

Supporting Information

ABSTRACT: Strong and stable visible-light-emitting boron nitride nanotube (BNNT)/biomolecule nanohybrids were successfully fabricated via noncovalent functionalization of BNNTs with flavin mononucleotides (FMN). Atomic force microscopy showed excellent dispersion of the nanohybrids in aqueous solution. Infrared absorption spectroscopy revealed strong $\pi-\pi$ stacking interactions between FMN and BNNT sidewalls. Importantly, the fluorescence spectra revealed that the nanohybrids were highly fluorescent in the visible-light spectral range. Moreover, this fluorescence had unique pH-dependent and thermally stable properties. These nanohybrids might be used to construct novel fluorescence imaging probes that function over a wide pH and temperature range.

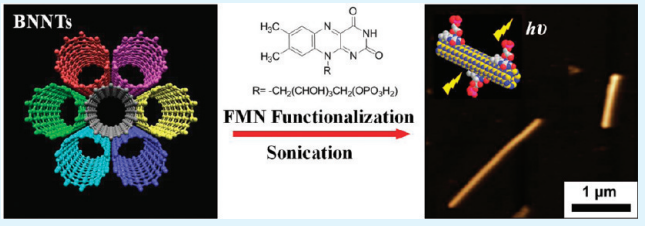

KEYWORDS: boron nitride nanotube, flavin mononucleotide, nanohybrid, functionalization, visible light emission

Over the past decades, one-dimensional (1D) nanoscale materials-based optics and optoelectronics have been considered valuable for potential applications in modern imaging techniques that utilize novel fluorescent tags for the analysis of atomic scale objects and visualization of single cells.[1] In particular, pH-dependent optics based on 1D nanoscale materials has just recently begun to attract attention, because they can be employed to trace pH-dependent biological and pathological processes, such as metabolism and neurotransmission.[2−5]

Boron nitride nanotubes (BNNTs) have an analogous structure to carbon nanotubes (CNTs), but have a stable and wide band-gap of 5.5 eV independent of tube diameter and chirality.[6−9] BNNTs exhibit superb thermal conductivity. They are chemically more stable than CNTs,[10] particularly at high temperatures and under oxygen-enriched atmospheres. Moreover, reportedly, BNNTs possess excellent biocompatibility with lower cytotoxicity as compared to CNTs when they are incubated with various cells.[11] Such unique properties make BNNTs an ideal nanoscale fluorescence material. In fact, the cathodoluminescence of both pristine BNNTs and those doped with rare-earth elements was investigated, and near-ultraviolet (UV) light emission was successfully observed.[12,13] Nanohybrid materials composed of BNNTs with biomolecules are thought to be a novel class of fluorescence materials.[14] Such novel nanohybrids should effectively function in oxidative or hazardous environments at high temperatures.

Flavin mononucleotide (FMN) is a well-known phosphorylated derivative of vitamin B_2. It plays an important role in numerous basic biological species as coenzymes and photoreceptors.[15] Its molecular structure consists of an aromatic isoalloxazine ring and a phosphate moiety. Recently, both theoretical and experimental studies have indicated that highly fluorescent, single-walled carbon nanotubes (SWNTs) hybrids can be obtained by organizing FMN molecules on the tube sidewalls via strong $\pi-\pi$ stacking interactions between the isoalloxazine rings and graphene-like tube surfaces, as well as via intermolecular hydrogen bonding between the isoalloxazine rings, thereby leading to the efficient individualization and chirality selection of SWNTs.[16−18] From these observations, we hypothesized that FMN molecules could interact with the hydrophobic surfaces of BNNTs in a similar way as in case of SWNTs. This would open a new, noncovalent, sidewall chemical pathway for not only solubilizing and functionalizing BNNTs in an aqueous phase, but also for further integration of these innovative BNNTs-based hybrids into new composite materials and devices.

In this paper, we report on the disentanglement of BNNTs in an aqueous phase via noncovalent functionalization of BNNTs with FMN molecules. Then pH-dependent and thermally stable fluorescence properties of these novel FMN/BNNT nanohybrids were studied. The nanohybrids showed bright and stable pH-dependent fluorescence properties in the visible light range.

Received: November 5, 2010
Accepted: February 18, 2011
Published: February 28, 2011

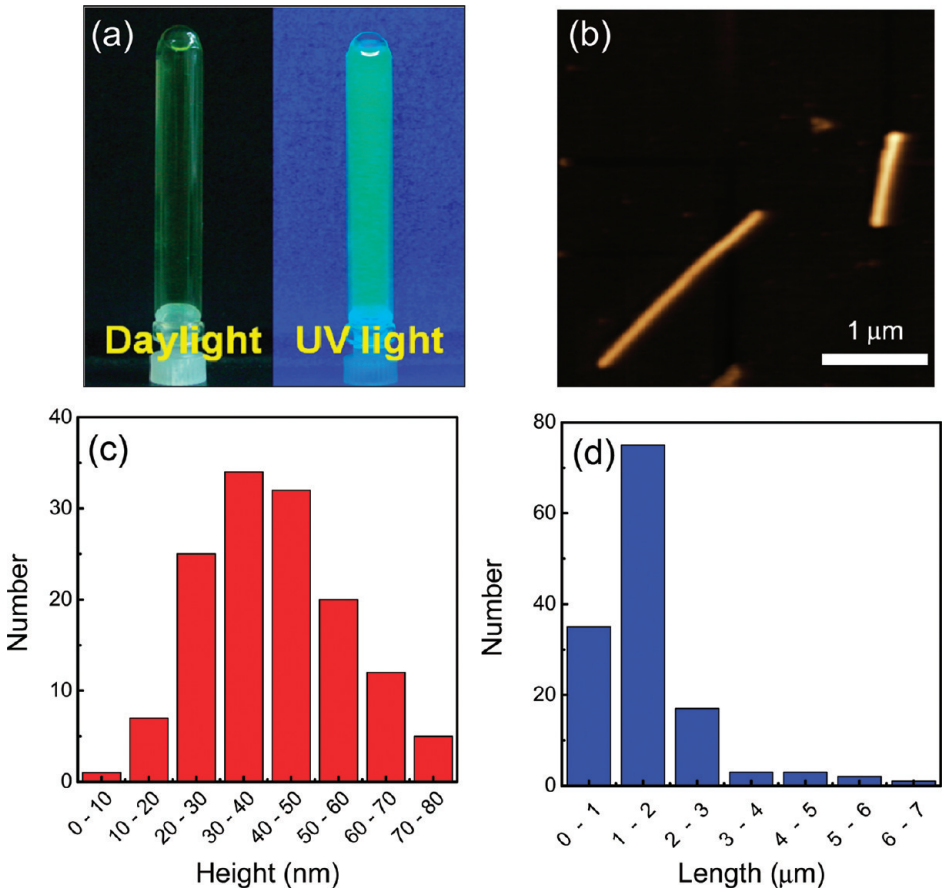

Figure 1. (a) Dispersion of FMN/BNNT nanohybrids in an aqueous solution under daylight and UV light (365 nm) excitations. (b) AFM image of the FMN/BNNT nanohybrids, and statistical analysis of (c) height and (d) length of the FMN/BNNT nanohybrids collected from 29 different AFM images (the total number of BNNTs was 136).

Scheme 1. Schematic Representation of the Formation Process of a FMN/BNNT Nanohybrid

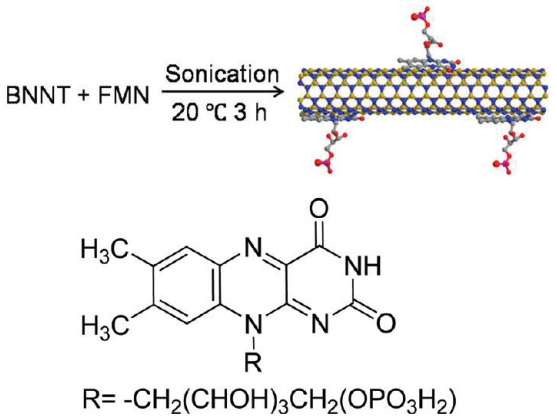

Herein we propose that this class of supramolecular 1D nanohybrids is a promising candidate for the next generation of photonic and optoelectric devices.

Highly pure multiwalled BNNTs were synthesized via a carbon free chemical vapor deposition method, as reported elsewhere.[19] In a typical functionalization procedure (Scheme 1), 1.5 mg of BNNTs were added into aqueous solutions containing 100 μM FMN in a total volume of 3 mL, and then the mixed solution was sonicated for 3 h, followed by centrifugation at 2000 rpm for 25 min to remove any insoluble BNNTs. Subsequently, we performed dialysis against milliQ water for 24 h to remove any unbound FMN molecules. The remaining solution was collected for further characterization. The solution was transparent yellow to turbid orange in color, and showed bright green fluorescence under UV light (365 nm) (Figure 1a). No precipitates were observed after incubation for a long time in an ambient environment. The experimental details are summarized in the Supporting Information.

The morphologies of the FMN/BNNT nanohybrids were then investigated by atomic force microscopy (AFM). The AFM images displayed excellent dispersion of rodlike objects on the mica surface (Figure 1b). To evaluate the diameter and length of these objects, we performed statistical analyses based on the AFM images (Figure 1c, d). The analyses indicated that the objects had heights of less than 80 nm and lengths of up to 8 μm, which are essentially consistent with those of the starting BNNTs.[20] However, the lengths were slightly shorter than in the case of original BNNTs (up to 10 μm); this difference may be due to partial tube shortening during the sonication procedure. These observations suggested that the observed rodlike objects represented the disentangled BNNTs well-dispersed via FMN functionalization in the aqueous phase.

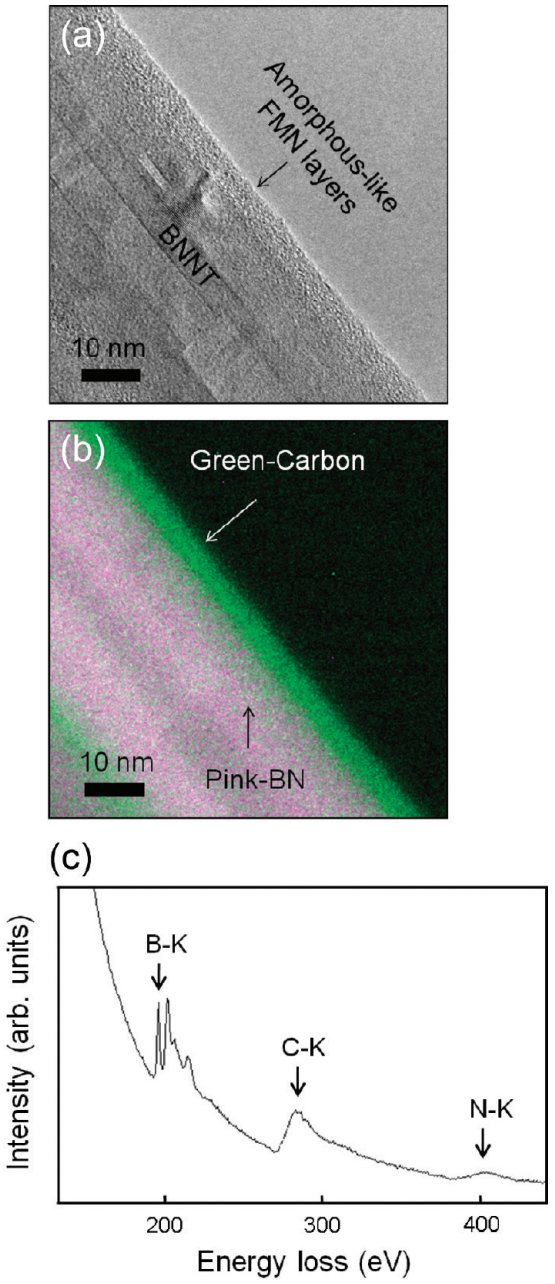

Figure 2. (a) HRTEM image, (b) corresponding spatially resolved elemental map, and (c) EEL spectrum of a representative FMN/BNNT nanohybrid.

The morphologies/structures of the FMN/BNNT nanohybrids were analyzed by high-resolution transmission electron microscopy (HRTEM). The images showed the presence of amorphous-like layers on the sidewalls of BNNTs, which were not present on the starting BNNTs (Figure 2a and the Supporting Information, Figure S1). This provides solid evidence that BNNTs were successfully functionalized with FMN. The distribution of FMN on BNNTs was further confirmed by constructing spatially resolved elemental maps using energy-filtering TEM. The overlay of BN, and C signal intensities showed highly enriched C contents on the BNNT periphery (Figure 2b), where FMN functionalization took place. In addition, the electron energy loss (EEL) spectra (Figure 2c) of the same nanohybrids

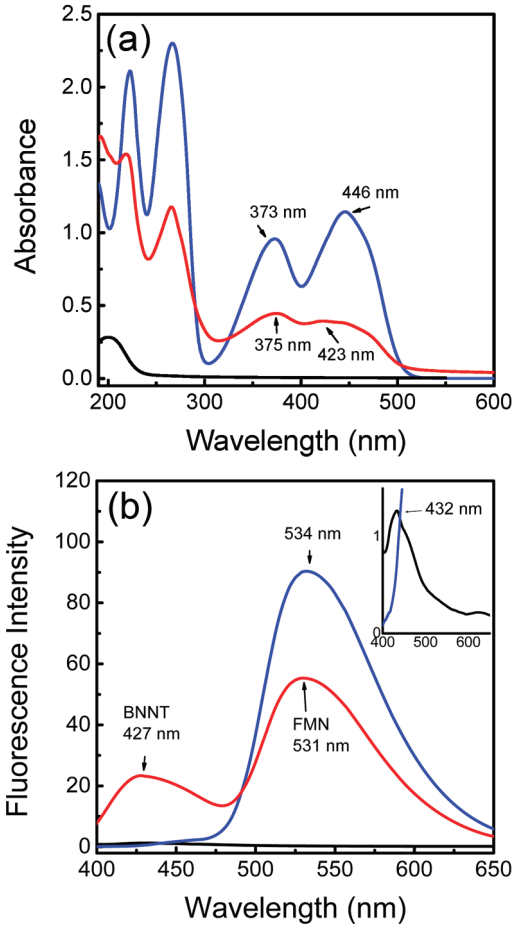

Figure 3. (a) Comparative UV/vis and (b) FS spectra of original BNNTs (black), pure FMN (blue), and FMN/BNNT nanohybrids (red). The inset shows enlarged FS spectra between 400 and 650 nm.

displayed the characteristic K-edges of C at 283 eV along with B at 198 eV and N at 401 eV. The appearance of C K-edge also supported the regarded functionalization of BNNTs with FMNs.

Fourier-transformed infrared absorption (FT−IR) spectroscopy was applied to gain insight into the functionalization mechanism (see Figure S2 in the Supporting Information). Specifically, the peaks derived from the original BNNTs appeared at 771 and 1347 cm^{-1}, which were assigned to the respective E1u (TO) and E1u (LO) modes (TO: transverse optic; LO: longitudinal optic),[21] whereas the peaks for the nanohybrids appeared at around 818 and 1379 cm^{-1}. Interestingly, the E1u (TO) modes of the nanohybrids were split into two peaks at 818 and 799 cm^{-1}. The inter-plane B−N bond strength must be weakened due to binding of the FMN molecules onto the BNNT surfaces. It is worth noting that the vibration band at 2950 cm^{-1} can be attributed to the υ_{as} (CH_2) of pure FMN, but appeared at 2922 cm^{-1} for the nanohybrids. The intensity of the υ_{as} (CH_2) for the nanohybrids was relatively stronger than that for pure FMNs. These observations suggest that intermolecular hydrogen bonds were formed among the adjacent isoalloxazine rings of FMN molecules on the sidewalls of the BNNTs.[16−18] Therefore, we concluded that the $\pi-\pi$ stacking interactions between FMN and BNNTs play a major role in our system, and the other interactions may also supply positive contributions.

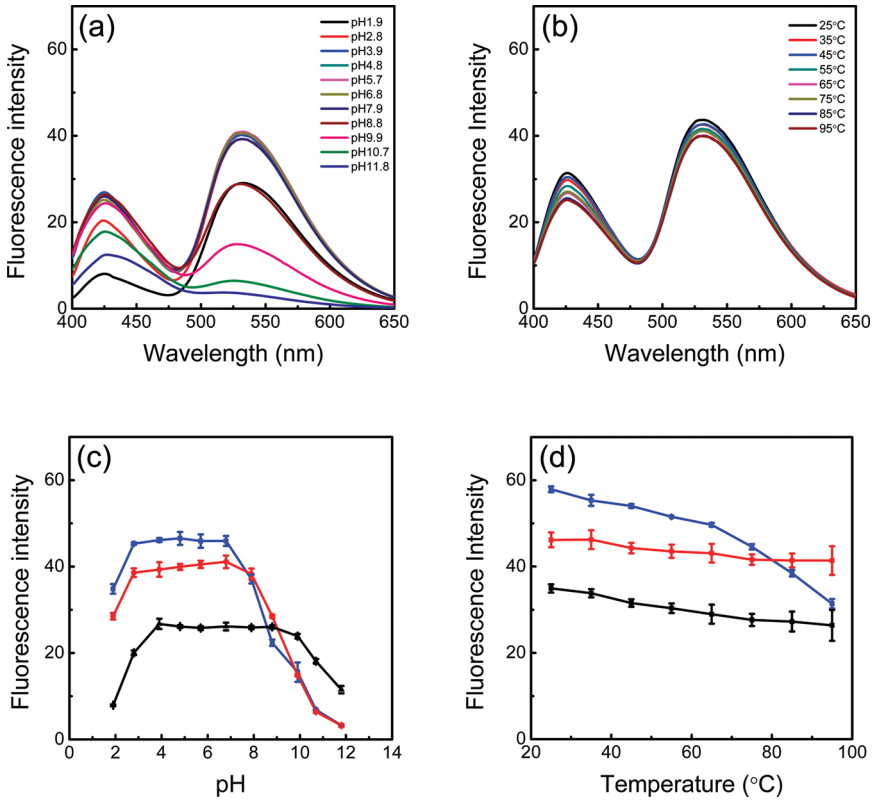

Figure 4. (a) pH and (b) temperature-dependent fluorescence of the FMN/BNNT nanohybrids. (c) Comparative pH and (d) temperature-dependent fluorescence intensity of pure FMN (blue), BNNTs in nanohybrids (black), and FMN in nanohybrids (red).

Ultraviolet−visible absorption (UV/vis) spectroscopy was employed to reveal the optical properties of the FMN/BNNT nanohybrids (Figure 3a). Four peaks were clearly observed at around 223, 267, 373, and 446 nm in the spectra of pure FMN, which were attributed to $\pi-\pi^*$ type transitions.[22,23] On the other hand, those peaks in the nanohybrids were slightly shifted to 218, 265, 375, and 423 nm, respectively. These changes strongly suggest that electron transfers, which originated from the strong $\pi-\pi$ stacking interactions, existed between the FMNs and BNNTs. It should be stressed that a small red shift of the peak at 373 nm can be attributed to the fact that intermolecular hydrogen bonds were formed between the adjacent isoalloxazine rings via self-assembly of the FMN molecules on the sidewalls of BNNTs, similar to the case of the FMN/CNT nanohybrids.[16−18]

Fluorescence spectroscopy (FS) is an ideal tool for evaluating the fluorescence properties of nanomaterials. In the spectra of the FMN/BNNT nanohybrids (Figure 3b) two bright fluorescent peaks were observed at 427 and 531 nm. They were attributed to the BNNTs and FMN, respectively. The former peak, which was attributed to B or N defect centers, or to radiative excitonic dark states of the BNNTs,[21] slightly blue-shifted from the peak of the original BNNTs at 432 nm. The latter peak was also blue-shifted compared with the peak for pure FMN at 534 nm. These observations suggest that both FMN molecules and BNNTs have different electronic states after hybrid formation. In fact, the fluorescence of the original BNNTs dispersed in the absence of FMN molecules was barely observed, indicating that the amount of BNNTs was drastically increased by FMN. Further investigation of the stability of the fluorescence was conducted by measuring the steady-state fluorescence of the FMN/BNNT nanohybrids as a function of time (see Figure S3 in the Supporting Information). The fluorescence intensity only marginally decreased with time in an air atmosphere, indicating that the fluorescence of the FMN/BNNT nanohybrids was sufficiently stable.

Nanomaterials with pH-dependent fluorescence properties have highly promising applications for monitoring pH-dependent biological processes.[2−5] Therefore, the properties of the FMN/BNNT nanohybrids were investigated to explore their future applicability in the biological field. As shown in panels a and c in Figure 4 (see Figure S4 in the Supporting Information for the UV/vis spectra), the fluorescence peak at 531 nm, which was attributed to the FMN molecules on the BNNT surface, displayed a unique pH-dependent behavior. This behavior was in a good agreement with the pH-dependent fluorescence of pure FMN. It is known that isoalloxazine rings exist in three redox states, which are cationic, neutral, and anionic structures, depending on the pH environment (Scheme 2). The normal form of the isoalloxazine ring in the ground state is neutral. This neutral FMN will transform into cationic and anionic species at pHs 3.5 and 9, respectively.[24] Accordingly, it was observed that the FMN molecules on the BNNT surface behaved similarly as free FMN.

The pH-dependent properties of the peak at 427 nm, which was attributed to the BNNTs in the nanohybrids, were more interesting. At neutral pH values (pH 3.9−8.8) the fluorescence intensity was strong and stable with changes in pH. At low (pH 1.9−3.9) and high pH (pH 8.8−11.8) the intensity became remarkably sensitive to pH changes. This behavior seems to be correlated with the different redox states of the FMN molecules. FMN molecules in the neutral state should have strong $\pi-\pi$ stacking interactions with BNNTs. At low and high pH values,

Scheme 2. Equilibrium of FMN between Cationic, Neutral, and Anionic Flavin Species

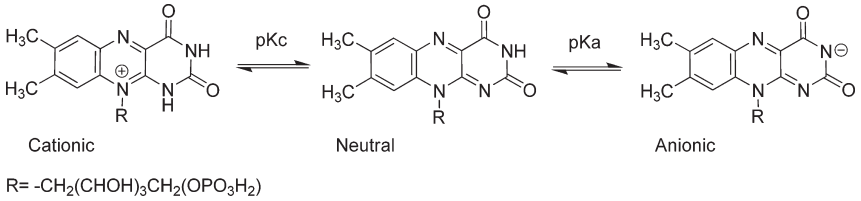

the FMN molecules on the BNNT surface should desorb due to relaxation of the $\pi-\pi$ stacking interactions, followed by fluorescence quenching due to the formation of BNNT bundles. Recently, Huang et al. developed a submicrometer-sized pH sensor based on Ag nanoparticle-decorated biotin−fluorescein/BNNT hybrids. The pH-dependent fluorescence and Raman signals in the fluorescein molecules enhanced by Ag nanoparticles allowed pH determination by comparing the fluorescence intensities or identifying the ratio of two typical Raman peaks. The sensor worked well within the pH 5.5−8.2 range, and was envisaged to be highly promising for monitoring the environmental pH of subunits in living cells.[25] In contrast, because the fluorescence intensity of the present FMN/BNNT nanohybrids was stable over the same pH range, these novel nanohybrids might be an alternative building block for designing novel fluorescence imaging probes, which would be able to work under circumstances where the effect of changes in pH on fluorescence must be eliminated.

Further investigation of the temperature-dependent fluorescence of the FMN/BNNT nanohybrids was conducted, as shown in Figure 4b, d (see Figure S5 in the Supporting Information for the UV/vis spectra). The fluorescence intensity of both peaks at 427 and 531 nm for the nanohybrids barely changed with temperature changes. On the other hand, the fluorescence intensity of pure FMN gradually decreased with temperature, indicating that the fluorescence of the FMN molecules on the BNNT surface was more stable than in its free state. In general, the fluorescence intensity of certain molecules is markedly quenched with increasing temperature, which is due to an increase in the rate constant for the nonradiative transitions.[26] Therefore, the nonradiative transitions were efficiently depressed in the nanohybrids.

In summary, we have demonstrated the preparation and characterization of novel FMN/BNNT nanohybrids. AFM observations have indicated that the nanohybrids possess excellent solubility and disentangled dispersion in an aqueous solution. The FT−IR spectra have suggested that strong interactions are present between the BNNT sidewalls and FMN molecules. These nanohybrids exhibit bright green fluorescence in the visible range. At the same time, the fluorescence intensity has unique pH-dependent and thermally stable properties. Although the differences between FMN/BNNT and FMN/CNT nanohybrids are needed to be clarified in the further studies, we propose that the present FMN/BNNT nanohybrids should be given considerable attention with respect to their utilization in visible light emitters or nanoscale subunits for constructing fluorescence imaging probes that can function over a wide temperature range.

■ ASSOCIATED CONTENT

Supporting Information. Additional figures (PDF). This material is available free of charge via the Internet at http://pubs.acs.org.

■ AUTHOR INFORMATION

Corresponding Author
*E-mail: t-serizawa@bionano.rcast.u-tokyo.ac.jp.

■ ACKNOWLEDGMENT

We thank Prof. H. Matsuno (Kyushu University) and Dr. T. Sawada (The University of Tokyo) for kind discussion. This work was supported in part by the Grant-in-Aid for Scientific Research (20350052 and 21106506).

■ REFERENCES

(1) Xia, Y.; Yang, P.; Sun, Y.; Wu, Y.; Mayers, B.; Gates, B.; Yin, Y.; Kim, F.; Yan, H. *Adv. Mater.* **2003**, *15*, 353–389.
(2) Han, J.; Burgess, K. *Chem. Rev.* **2010**, *110*, 2709–2728.
(3) Lee, M.; Gubernator, N. G.; Sulzer, D.; Sames, D. *J. Am. Chem. Soc.* **2010**, *132*, 8828–8830.
(4) Hong, C.; Pan, C. *J. Mater. Chem.* **2008**, *18*, 1831–1836.
(5) Hartman, K. B.; Laus, S.; Bolskar, R. D.; Muthupillai, R.; Helm, L.; Toth, E.; Merbach, A. E.; Wilson, L. *Nano Lett.* **2008**, *8*, 415–419.
(6) Chopra, N. G.; Luyken, R. G.; Cherrey, K.; Crespi, V. H.; Cohen, M. L.; Louie, S. G.; Zettl, A. *Science* **1995**, *269*, 966–967.
(7) Golberg, D.; Bando, Y.; Tang, C.; Zhi, C. Y. *Adv. Mater.* **2007**, *19*, 2413–2432.
(8) Blase, X.; Rubio, A.; Louie, S. G.; Cohen, M. L. *Europhys. Lett.* **1994**, *28*, 335–340.
(9) Golberg, D.; Bando, Y.; Huang, Y.; Terao, T.; Mitome, M.; Tang, C.; Zhi, C. Y. *ACS Nano* **2010**, *4*, 2979–2993.
(10) Xiao, Y.; Yan, X.; Cao, J.; Ding, J.; Mao, Y.; Xiang, J. *Phys. Rev. B* **2004**, *69*, 205415−1–5.
(11) Chen, X.; Wu, P.; Rousseas, M.; Okawa, D.; Gartner, Z.; Zettl, A.; Bertozzi, C. R. *J. Am. Chem. Soc.* **2009**, *131*, 890–891.
(12) Zhi, C. Y.; Bando, Y.; Tang, C.; Golberg, D.; Xie, R.; Sekiguchi, T. *Appl. Phys. Lett.* **2005**, *86*, 213110−1–3.
(13) Chen, H.; Chen, Y.; Li, C. P.; Zhang, H.; Williams, J. S.; Liu, Y.; Liu, Z.; Ringer, S. P. *Adv. Mater.* **2007**, *19*, 1845–1848.
(14) Gao, Z.; Zhi, C. Y.; Bando, Y.; Golberg, D.; Serizawa, T. *J. Am. Chem. Soc.* **2010**, *132*, 4976–4977.
(15) Massey, V. *Biochem. Soc. Trans.* **2000**, *28*, 283–296.
(16) Lin, C.; Zhang, R.; Niehaus, T. A.; Frauenheim, T. *J. Phys. Chem. C* **2007**, *111*, 4067–4073.
(17) Yu, S. Y.; Papadimitrakopoulos, F. *J. Am. Chem. Soc.* **2008**, *130*, 655–664.
(18) Yu, S. Y.; Doll, J.; Sharma, I.; Papadimitrakopoulos, F. *Nat. Nanotechnol.* **2008**, *3*, 356–362.
(19) Zhi, C. Y.; Bando, Y.; Tang, C.; Golberg, D. *Solid State Commun.* **2005**, *135*, 67–70.
(20) Zhi, C. Y.; Bando, Y.; Tang, C.; Xie, R.; Sekiguchi, T.; Golberg, D. *J. Am. Chem. Soc.* **2005**, *127*, 15996–15997.
(21) Zhi, C. Y.; Bando, Y.; Tang, C.; Honda, S.; Sato, K.; Kuwahara, H.; Golberg, D. *Angew. Chem., Int. Ed.* **2005**, *44*, 7932–7935.
(22) Grajek, H.; Drabent, R.; Żurkowska, G.; Bojarski, C. *Biochim. Biophy. Acta* **1984**, *801*, 456–460.

(23) Mortland, M. M.; Lawless, J. G.; Hartman, H.; Frankel, R. *Clays Clay Miner.* **1984**, *32*, 279–282.
(24) Drössler, P.; Holzer, W.; Penzkofer, A.; Hegemann, P. *Chem. Phys.* **2002**, *282*, 429–439.
(25) Huang, Q.; Bando, Y.; Zhao, L.; Zhi, C. Y.; Golberg, D. *Nanotechnology* **2009**, *20*, 415501−1–6.
(26) Grajek, H.; Żurkowska, G.; Bojarski, P.; Kukliński, B.; Smyk, B.; Drabent, R.; Bojarski, C. *Biochim. Biophy. Acta* **1998**, *1384*, 253–267.